

## MULTI-RESOLUTION IMPERVIOUS SURFACE MAPPING FOR IMPROVED RUNOFF ESTIMATION AT CATCHMENT LEVEL

*Tim Van de Voorde<sup>1</sup>, Jaroslaw Chormanski<sup>2\*</sup>, Okke Batelaan<sup>2</sup> and Frank Canters<sup>1</sup>*

1. Vrije Universiteit Brussel, Department of Geography, Brussels, Belgium; tvdvoord@vub.ac.be
  2. Vrije Universiteit Brussel, Department of Hydrology and Hydraulic Engineering, Brussels, Belgium; batelaan@vub.ac.be
- \*. Current address: Department of Hydraulic Structures and Environmental Restoration, Warsaw Agricultural University, Warsaw, Poland

### ABSTRACT

In this paper, a multi-resolution approach is presented for mapping surface imperviousness in urbanised areas. The approach involved two steps. First, a detailed land-cover map was produced from a high resolution (HR) Ikonos image that covers part of the Brussels metropolitan area. The output of the classification was improved with post-classification techniques. This enhanced HR classification of a relatively small area was then used to train a neural network based sub-pixel classification model that estimates impervious surface cover proportions within the pixels of a medium-resolution (MR) Landsat ETM+ image that covers the entire agglomeration of Brussels.

Both the HR and the MR map were used as input to a rainfall-runoff simulation on the upper catchment of the Woluwe River. Three alternative land-cover scenarios were tested: one for which a single impervious surface coefficient was defined for all urban classes, a second in which separate coefficients were derived for different types of urban morphology and finally, a spatially fully distributed scenario was applied where each cell in the simulation model was assigned its own coefficient based on the HR and MR maps of imperviousness.

The study points to some interesting conclusions: it shows that estimates derived from satellite data may strongly differ from those made by experts for some urban classes, that the use of spatially distributed land-cover information obtained from satellite derived maps produces higher peak discharges, and little difference was observed between results obtained with detailed impervious surface maps derived from HR data and sub-pixel estimates derived from MR data. This proves that multi-resolution methods, which provide information on surface imperviousness for areas of large extent at relatively low cost, may be an interesting alternative for expensive HR mapping for rainfall-runoff modelling at catchment level.

### INTRODUCTION

Continuing worldwide urban growth increases the amount of impervious surfaces of man-made materials, which change the hydrological properties of a watershed: instead of gently infiltrating, surface water will runoff to the rivers more quickly, picking up potentially polluting substances on its way. This in turn increases the risk for water pollution and floods in the watershed, requires the construction of expensive water purification systems, hampers the recharging of aquifers and boosts erosion (Arnold & Gibbons, 1996; Schueler, 1994).

Numerous methods have been proposed for impervious surface mapping, many of which rely on existing land-use datasets (Prisloe et al., 2000; Sleavin et al., 2000; Cain, 2004). These so-called indirect methods associate a percentage of imperviousness with each land-use type. The drawback of this approach is that there is no standardized method for deriving these coefficients and that there may be a high variability in the amount of imperviousness within the same land-use class. If mapping at a spatially more detailed level is required, a direct approach is preferred (Cain, *ibid.*). This involves deriving impervious surfaces directly from aerial photographs or satellite im-

ages. Satellite images are especially well suited for mapping impervious surfaces (Slonecker et al., 2001). In comparison with alternative data sources such as aerial photographs, they have a larger spatial extent, a relatively fast repeat cycle and are competitively priced. There is a wide range of satellite data types available on the market that could be used for impervious surface mapping. In general terms, impervious surface information could be extracted directly from any land-cover classification derived from satellite imagery. The cost, in terms of data requirements and effort, the accuracy of the end-product and the feasibility of the project, however, will be largely dependent on the selected satellite data type. For instance, it will be difficult in practice to obtain a complete and cloud-free coverage for larger areas when using high resolution (HR) images (type Ikonos, Quickbird) for land-cover mapping because of the relatively small footprint of this type of images. Furthermore, this method would also be very cost-intensive, especially when frequent updates are required. On the other hand, satellite data with a lower spatial resolution (i.e. medium resolution data - MR) are cheaper and offer greater spatial extent but also provide less spatial detail, which may lead to a product that does not meet customer requirements.

Sub-pixel classification techniques offer the opportunity to combine the advantages of satellite images with different spatial resolutions by exploiting the relationship between the spectral signatures of pixels in a high resolution image and the proportions of land-cover classes present within these pixels, which are in turn derived from a HR land-cover classification. This method can therefore create synergy by retaining the large spatial extent of MR satellite platforms while making optimal use of the spatial detail provided by HR satellite platforms.

Several techniques for sub-pixel impervious surface mapping have already been examined: Yang et al. (2003) applied decision trees, Ji and Jensen (1999) used spectral unmixing, and Wang et al. (2000) and Flanagan and Civco (2001) employed artificial neural networks (ANN). The purpose of our research is to use sub-pixel classification driven by an ANN to estimate the proportions of four land-cover classes (bare soil, impervious surfaces, water and vegetation) within Landsat ETM+ pixels using a land-cover classification derived from an overlapping VHR Ikonos image as reference data. The ANN learns the relationship between the spectral information of the ETM+ pixels and the proportions of the four land-cover classes within each pixel from a randomly selected training set of ETM+ pixels for which the corresponding class proportions are derived from the HR land-cover classification. Once a reliable ANN model is obtained, it can be applied on any ETM+ pixel, including those for which no HR land-cover classification is available. To this end, we developed and compared two ANN sub-pixel models: a first model only has the multispectral ETM+ channels as input variables and a second model combines the multispectral channels with the band-ratios of each channel (e.g. band1/band3).

The performance of these models will be heavily dependent on the quality of the input data. Errors will occur when the land-cover class composition of ETM+ pixels is different from that of the constituent Ikonos pixels. This may occur for three reasons: (1) the two images are not well geometrically aligned, (2) the HR classification contains errors, and (3) land-cover changes have occurred between the acquisition dates of the ETM+ and Ikonos images. These issues were taken into account before we developed our models: care was taken to assure a good co-registration between the ETM+ and the Ikonos image, post-classification techniques were applied to improve the quality of the HR reference classification, and temporal differences between the two images were accounted for by applying temporal filtering on the data samples.

## **METHODS**

### **Developing the reference land-cover classification**

We used an ANN to build the reference land-cover classification, which consists of 11 classes: light and dark red surfaces, light, medium and dark grey surfaces, bare soil, water, crops, shrub and trees, grass, and shadows. This neural network was created with Neuralware's NeuralWorks Predict® software. The accuracy of the resulting land-cover map was assessed with independent validation data.

Training data for this classification were obtained by digitizing about 200 random training pixels per class on the Ikonos image. As an independent validation set, we chose a stratified random sample: the amount of pixels to be sampled in each class depended on the class's prominence in the image. With the training data, neural network models were built according to 4 scenarios. Each type of network had a different combination of input variables: only the multi-spectral bands, the multi-spectral bands with the PAN band, the multi-spectral bands with the PAN band and a vegetation index (NDVI), and the multi-spectral bands with PAN, NDVI and 2 texture measures. The texture measures we used were local variance and binary comparison matrix (Murphy, 1985). Transformations of the input bands and a selection according to their relative contribution to the overall information content were accomplished with NeuralWorks Predict®. The transformed input variables that were retained in each scenario to actually perform the classification were chosen from a set of 5 mathematical transformations per original input band using a genetic-based variable selection algorithm embedded in the software.

The success of our sub-pixel classification strategy depends heavily on obtaining reliable training data, i.e. accurate land-cover proportions for each ETM+ training pixel. Because many potential sources of bias were present in the resulting land-cover map, we improved its accuracy and coherence with several post classification techniques: shadow removal, structural filtering (Barr and Barnsley, 2000) and correction of classification errors with knowledge-based rules. To this end, we adopted the method and workflow suggested by Van de Voorde et al. (2004, 2006). The 11 classes were aggregated afterwards to a single vegetation class (including shrub and trees, grass and crops), a single "impervious surfaces" class (including red and grey surfaces) and the classes water and bare soil.

### **Subpixel classification**

Once reliable reference data were obtained, we could build neural network models for sub-pixel classification with a random sample of high resolution pixels, which were drawn from the part of the image that overlaps the HR classification. Each sample point consisted of the spectral values of the ETM+ pixel and the proportion of the four target classes (bare soil, built-up surfaces, water and vegetation) within this pixel.

Because it will be very difficult in practice to obtain MR and HR images of the same dates, it is likely that land-cover changes are present in the images used in a multi-resolution approach. These changes may be seasonal (leaf-on versus leaf-off for deciduous trees, crop cycles) or point to actual land-use changes (e.g. urban growth). To remove changed pixels from the random sample of HR pixels, we assumed that the Normalized Difference Vegetation Index (NDVI) of the HR pixels shows a clear relationship with the average NDVI of the constituent HR pixels and applied a non-linear regression to remove outlying pixels. In doing so, we had to take into account that the digital numbers (DN), which represent the spectral response from the visible red and near infrared channels required to calculate NDVI, originate from two different sensor platforms. To account for this, they were converted to in-band radiance at sensor aperture. This was achieved with the equations proposed by Taylor (2005) for the Ikonos images and by Irish (2000) for the ETM+ image.

Two models were then built with NeuralWare's Predict software and compared independently. These models differed in the type of input variables, i.e. spectral channels that were used. The first model had the six ETM+ multispectral bands as input (bands 1-5 and band 7). The second model included all possible ratios between the spectral channels in addition to the multispectral channels.

The performance of the models was assessed by applying them on an independent validation set to estimate the proportions of each of the four classes. The total mean absolute error (TMAE) was used to assess the overall accuracy of the proportion estimation. The TMAE is calculated by making the sum of the per-class mean absolute errors (MAE) of each target class, which are in turn derived by taking the mean of the absolute values of the difference between predicted and reference proportions of all validation samples. The per-class MAE can be interpreted as an error percentage, while the TMAE is a more general error measure, only suitable to mutually compare different models. Because it is the sum of the per-class MAE's, its value lies between 0 (no error) and 2 (maximum possible error) and it cannot be interpreted as a percentage.

## Run-off simulation

Both the HR and the MR map were used as input for a rainfall-runoff simulation of the Upper-Woluwe catchment, located in the south-eastern part of Brussels. Three alternative land-cover scenarios were tested. First, one single impervious surface coefficient was defined for all urban classes based on expert judgement and on calculation of an average level of imperviousness from the HR and MR classification results. Next, separate coefficients were derived for different types of urban morphology. Finally, a spatially fully distributed scenario was applied where each cell in the simulation model was assigned its own coefficient based on the HR and MR maps of imperviousness.

A modelling approach with hourly time step was used for the rainfall-runoff simulation for the Upper Woluwe catchment. The applied WetSpa (Water and energy transfer between soil, plants and atmosphere) distributed GIS-based hydrological model predicts peak discharges and hydrographs and simulates the spatial distribution of catchment hydrological characteristics, based on hydrometeorological data and distributed maps of topography, soil type, and land cover (Liu and De Smedt, 2005).

## RESULTS

### Accuracy of the reference classification

The pixel-based classification of the Ikonos image was obtained by training and comparing several neural networks. The best performing network consisted of 9 inputs, 17 hidden nodes and 11 output nodes (i.e. the 11 land-cover classes). The input variables were mathematical transformations of the red, green and blue image bands, the NDVI and two texture measures, namely standard deviation and binary comparison matrix. The overall performance of this network on an independent validation set of 2243 samples was characterized by a kappa index-of-agreement of 0.91.

Despite the relatively high numeric accuracy of the classification result, many problems such as shadow, structural clutter and classification errors remained. The first step in improving the classification was to remove the shadow pixels using the technique described in Van de Voorde et al. (2006). In this approach, shadows are reclassified with a separate neural network that was trained with the activation levels of the network that was used to make the land-cover classification. Approximately 56% of the separate set of shadow validation samples was correctly re-assigned to a new class with the ANN-based shadow reclassification. This obviously introduces new errors, but also increases the information content of the classification, i.e. the shadows are removed. The newly introduced errors can be solved with other post-classification techniques. The second step of the post-classification enhancement consists of applying knowledge based rules to correct classification errors and a structural filter to reduce structural clutter. In total, 14 rules were developed and applied on the land-cover classification after shadow removal. An example of such a rule is shown below:

*- pixels belonging to <crop> regions that are adjacent to <shrub and trees> or <grass> and that are smaller than 1400 pixels, are assigned to their second most probable class if this class is either <shrub and trees> or <grass>, otherwise they are changed into the class to which they are most connected with.*

The kappa index, which was calculated on the same validation set, increased from 0.91 to 0.95 after post-classification.

### Temporal filtering

In order to obtain a neural network that will be used for sub-pixel classification, temporally filtered training and validation samples are required. A total of 9 650 samples was randomly selected on the part of the ETM+ image that overlaps with the Ikonos classification. For each of these samples,

the NDVI and the average NDVI of the Ikonos pixels that belong to it were calculated, using the spectral radiance values. The correlation coefficient between these two variables was 0.87.

To remove changed pixels, a quadratic function was fit to the data with the least-squares method, and the residuals of the sample points were examined. Samples whose residual value was larger than two times the standard deviation of all residuals were deleted. When this procedure was applied a first time, 410 samples were removed and the correlation increased to 0.92. After a second iteration, 8856 pixels remained with a correlation of 0.94. Further iterations provided no significantly better result.

The 8856 pixels that remained after temporal filtering were randomly split in 2048 training and 6808 validation samples. These two datasets were used respectively for training and validating the neural network models for each of the two scenarios.

### Sub-pixel classification

To begin with, we developed a model on temporally filtered data to predict proportions of the four target classes using only mathematical transformations of the ETM+ bands as actual input to the network. These transformations are required to scale the input data to values between 0 and 1, and the function used to achieve this (linear, exponential...) influences the training process. The genetic algorithm based variable selection embedded in Predict was used to determine which transformations were best suited for a particular model.

*Table 1: total mean absolute error (TMAE) and mean absolute error for each target class*

	BARE	IMPERVIOUS	VEGETATION	WATER	TMAE
With temporal filtering and without band ratios	0.057	0.094	0.099	0.029	<b>0.279</b>
Without temporal filtering and without band ratios	0.065	0.111	0.122	0.004	<b>0.302</b>
With temporal filtering and with band ratios	0.057	0.090	0.094	0.018	<b>0.259</b>

The performance of this first neural network model on the validation data is shown in the top row of table 1. Both the per-class mean absolute errors (MAE) and the total mean absolute error (TMAE) are shown. The per-class MAE's can be interpreted as an average error percentage, i.e. the mean magnitude of the estimation error. For example, the error made in estimating the amount of impervious surfaces within a validation pixel was 9.4% on average. For vegetation, the error was slightly higher ( $\pm 10\%$ ). The per-class mean errors (predicted minus reference, i.e. no absolute value), which provide a global view of the model's bias, were very close to zero for each class. This means that there is no systematic bias and that the errors will compensate each other if the model is used to produce aggregated statistics of larger areas, e.g. calculate the percentage imperviousness for an entire watershed.

The second row of table 1 shows the errors obtained with a neural network based on the same selection of input variables, but trained on samples that were not temporally filtered. As can be seen from the table, this increased the TMAE from 0.279 to 0.302. The per-class MAE's for vegetation and impervious surfaces each rise with about 2 percentage points. The following experiment will therefore be conducted on temporally filtered data and compared with the first experiment, outlined above.

In the second experiment (ANN2), all unique band-ratios of the six multispectral channels (15) were added to the input, bringing the total number of potential variables to 21. Mathematical transformations were calculated, and again the variable selection algorithm was used to withhold variables with meaningful information content. The neural network that resulted from this setup had 9 inputs, 0 hidden nodes and 4 output nodes. The transformed input channels that were withheld by

the variable selection included the following bands or band ratios: band 4; ratio 1/5, 2/5 (2 transforms), 2/7 (2 transforms), 3/4 (2 transforms) and 4/7.

When this model was applied to the validation data, the TMAE slightly decreased from 0.279 to 0.259 (table 1). This improvement can be attributed for the largest part to the drop of the MAE of the class "water". Prediction of impervious surfaces and vegetation improved only slightly.

Figure 1(a) shows an impervious surface map produced by ANN2 on the ETM+ data, corresponding to the spatial extent of the Ikonos image. This figure can be compared to figure 1(b), which shows an impervious surface map of the same area, derived directly from the VHR classification, but with proportions aggregated to 30 meter resolution. From the map highlighting the errors, i.e. predicted minus reference proportions (fig. 1(c)), it becomes apparent that the model underestimates the amount of impervious surfaces within pixels inside the dense urban centre. This may indicate that high proportions of impervious surfaces are estimated lower by the model.

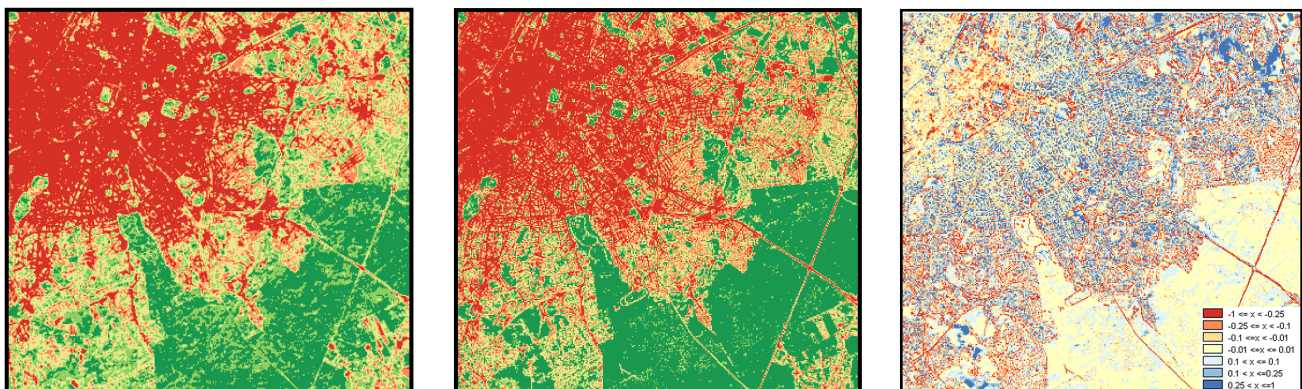


Figure 1: detail of the impervious surface map of Brussels for the part that overlaps with the Ikonos image (a); same detail derived directly from the Ikonos land-cover classification (b); map showing the differences between the two previous maps (predicted – reference) (c).

### Run-off

In the first, non-distributed scenario, the estimated impervious percentages were similar: 44% and 46% for respectively the HR and MR image. This is a significant difference compared to the standard expert judgement of 30% imperviousness. The simulated discharge peaks are 10-20% higher in the scenario with the HR image estimated average runoff coefficient than in case of expert judgement runoff coefficient. In the second scenario, with semi-distributed adjustment, differences between hydrographs simulated using HR and MR are very small. The runoff hydrograph in this scenario is slightly higher than in scenario one, based on an average impervious value determined by use of HR. Runoff simulated in the fully spatial distributed scenario and based on HR data gives very similar, but slightly higher discharges than in case of MR data. Compared to the non-distributed scenario, the maximum peaks in the distributed scenario are about 10% higher. This shows that for runoff simulation it is evidently important to know what the impervious percentage in the urban area is. However, it is even more important to derive its spatial distribution.

Figure 2 presents a comparison of simulated hydrographs for all scenarios of imperviousness distribution elaborated in this study: scenario 1, non-distributed with a priori guessed average imperviousness percentage value of 30%; scenario 1, non-distributed average imperviousness percentage of 44% calculated from Ikonos; scenario 2, semi-distributed for different classes and imperviousness percentage calculated from Ikonos and Scenario 3, fully-distributed per cell spatially varied imperviousness percentage. Analysed hydrographs show a relation between the level of impervious area and distribution versus simulated peak-discharges. The highest discharges are always simulated for the fully-distributed scenarios and the lowest for non-distributed ones. Increased connectivity of high runoff generating urban zones in the fully distributed scenario explain the higher peak discharges in this scenario and the need for distributed impervious estimates.

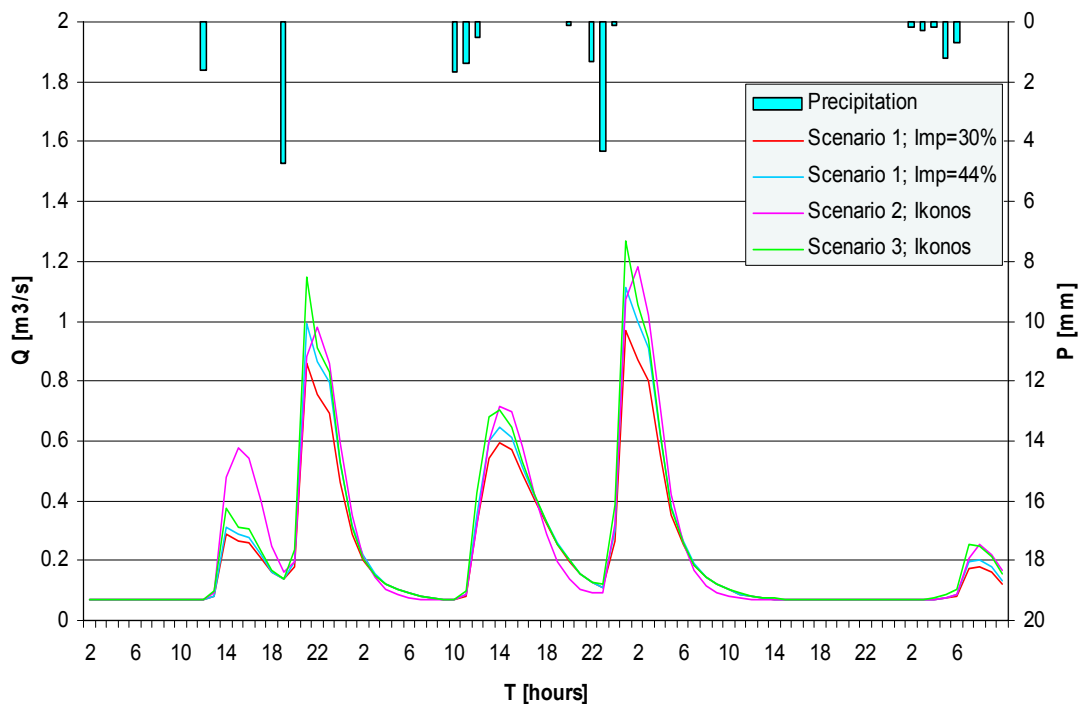


Figure 2: comparison of hydrographs simulated for 3 scenarios by using Ikonos data. Simulation period from 3<sup>rd</sup> of May 2005 1.00 am to 6<sup>th</sup> of May 2005 9.00 am.

## CONCLUSIONS

The first goal of this research was to develop and test a strategy for impervious surface mapping based on neural network driven sub-pixel classification of a Landsat ETM+ image, using an Ikonos land-cover classification to collect reference proportions for 4 target land-cover classes. To achieve this, we first required a reliable reference classification. A land-cover map consisting of 11 classes was made using a pixel-based neural network classifier. Because many problems related to shadows, noise and classification errors were present, post classification techniques were applied and succeeded not only in improving the visual appearance of the land-cover map, but also its overall kappa index (from 0.91 to 0.95). Then, two sub-pixel classification models were developed using the land-cover map to derive reference proportions for training and validation purposes. A first model (ANN1) was based on the multispectral data available in the ETM+ image. The positive effect of temporal change filtering, necessary to eliminate changed pixels from training and validation data was shown by a decrease of the total mean absolute error of nearly 8% when filtered samples were used. For the second model (ANN2), band ratios of the six multispectral ETM+ channels were added to the training data. This also proved to have a positive impact as the error further decreased with nearly 7%. Using the ANN2 model, sub-pixel impervious surface maps were derived for the entire subset of the ETM+ image, including those parts that were not covered by the Ikonos image from which the reference land-cover map was derived.

In the second part of the research, both the HR and the MR map were used as input for a rainfall-runoff simulation on the Woluwe upper catchment, located in the south-eastern part of Brussels. Three alternative land-cover scenarios were tested: one for which a single impervious surface coefficient was defined for all urban classes, a second in which separate coefficients were derived for different types of urban morphology and finally, a spatially fully distributed scenario was applied where each cell in the simulation model was assigned its own coefficient based on the HR and MR maps of imperviousness.

The study shows that although expert estimations of average imperviousness are reasonable, estimates derived from satellite data may strongly differ from expert knowledge for some urban classes, leading to substantially different estimates of discharge at catchment level. Furthermore,

the use of spatially distributed land-cover information obtained from satellite derived maps proves to produce higher peak discharges compared to scenarios based on the use of average levels of imperviousness for each land-use class. Little difference was observed between results obtained with detailed impervious surface maps derived from HR data and with sub-pixel estimates of imperviousness derived from MR data. This proves that multi-resolution methods, which provide information on surface imperviousness for areas of large extent at relatively low cost, may be an interesting alternative for expensive HR mapping for rainfall-runoff modelling at catchment level.

Future research will focus on assessing the robustness of the sub-pixel models by applying them on other parts of the same ETM+ image from which the subset in this study was extracted. The near-zero global error biases show that this may provide promising results. We will also continue to compare the sensitivity of runoff models to impervious surface maps developed with different techniques and input data, e.g. the sub-pixel technique described in this paper versus direct extraction of information on surface imperviousness from HR data.

## ACKNOWLEDGEMENTS

The authors wish to express their gratitude to Tim De Roeck of the Centre for Cartography and GIS (Vrije Universiteit Brussel) for his part in the work on impervious surface mapping. Belgian Science Policy is gratefully acknowledged for providing the funds for this research. The second author also acknowledges the support of the Research in Brussels programme for a post-doctoral fellowship.

## REFERENCES

- Arnold, C.A. Jr. and C.J. Gibbons, 1996. Impervious surface coverage: the emergence of a key urban environmental indicator. Journal of the American Planning Association, 62(2): 243-258
- Barr, S.L. and M.J. Barnsley, 2000. Reducing structural clutter in land cover classifications of high spatial resolution remotely-sensed images for urban land use mapping. Computers and Geosciences, 26(4): 433-449
- Cain, A., 2004. The usefulness of impervious cover mapping and analysis based on pre-existing classified land use datasets. In: the 2004 IMAGIN annual conference, URL: <http://www.imagin.org/awards/sp2004/Cain.pdf>, IMAGIN, East Lansing, Michigan (last date accessed : 3 August 2005)
- Flanagan, M. and D.L. Civco, 2001. Subpixel impervious surface mapping. In: proceedings of the ASPRS 2001 Annual Conference, St. Louis, MO. (American Society for Photogrammetry and Remote Sensing, Bethesda, Maryland), unpaginated CD-ROM
- Irish, R. R., 2000. Landsat 7 Science Data Users Handbook, Report 430-15-01-003-0, National Aeronautics and Space Administration, Goddard Space Flight Center, Maryland, URL: [http://ftpwww.gsfc.nasa.gov/IAS/handbook/handbook\\_toc.html](http://ftpwww.gsfc.nasa.gov/IAS/handbook/handbook_toc.html) (last date accessed: 30 November 2005)
- Ji, M. and J.R. Jensen, 1999. Effectiveness of subpixel analysis in detecting and quantifying urban imperviousness from Landsat Thematic Mapper imagery. Geocarto International, 14(4): 33-41
- Liu, Y.B. and F. De Smedt, 2005. Flood modeling for complex terrain using GIS and remote sensed information. Water Resources Management, 19: 605-624
- Murphy, D.L., 1985. Estimating Neighborhood Variability with a Binary Comparison Matrix. Photogrammetric Engineering and Remote Sensing, 51(6):667-674
- Prisloe, M., L. Gianotti and W. Sleavin, 2000. Determining impervious surfaces for watershed modeling applications. In: proceedings of the 8th national nonpoint source monitoring workshop. (Hartford, Connecticut)
- Schueler, T.R. 1994. The importance of imperviousness. Watershed Protection Techniques, 1(3): 100-110

- Sleavin, W.J., D.L. Civco, S. Prisloe and L. Gianotti, 2000. Measuring impervious surfaces for non-point source pollution modeling. In: proceedings of the ASPRS 2000 Annual Conference, Washinton, DC. (American Society for Photogrammetry and Remote Sensing, Bethesda, Maryland), unpaginated CD-ROM
- Slonecker, E.T., D.B. Jennings and D. Garofalo ,2001. Remote sensing of impervious surfaces: a review, Remote Sensing Reviews, 20(3): 227-255
- Taylor, M., 2005. Ikonos Planetary Reflectance and Mean Solar Exoatmospheric Irradiance, Space Imaging Inc., Thornton, Colorado URL: [http://www.spaceimaging.com/whitepapers\\_pdfs/Esun1.pdf](http://www.spaceimaging.com/whitepapers_pdfs/Esun1.pdf) (last date accessed: 30 November 2005)
- Van de Voorde, T., W. De Genst, F. Canters, N. Stephenne, E. Wolff and M. Binard, 2004. Extraction of land use/land cover related information from very high resolution data in urban and suburban areas. In: Remote Sensing in Transition. Proceedings of the 23rd Symposium of the European Association of Remote Sensing Laboratories, edited by R. Goossens (Millpress, Rotterdam), 237-244
- Van de Voorde, T., W. De Genst and F. Canters, 2006. Improving pixel-based VHR land-cover classifications of urban areas with post-classification techniques. Photogrammetric Engineering and Remote Sensing, accepted
- Wang, Y. and X. Zhang, 2004. A SPLIT model for extraction of subpixel impervious surface information. Photogrammetric Engineering and Remote Sensing, 70(7): 821-828
- Yang, L., C. Huang, C.G. Homer, B.K. Wylie, and M. J. Coan, 2003. An approach for mapping large-area impervious surfaces: synergistic use of Landsat-7 ETM+ and high spatial resolution imagery, Canadian Journal of Remote Sensing, 29(2): 230-240